

# Surface states on a topologically non-trivial semimetal: The case of Sb(110)

Marco Bianchi,<sup>1</sup> Dandan Guan,<sup>1,2</sup> Anna Stróżecka,<sup>3</sup> Celia H. Voetmann,<sup>1</sup>  
Shining Bao,<sup>2</sup> Jose Ignacio Pascual,<sup>4</sup> Asier Eiguren,<sup>5,6</sup> and Philip Hofmann<sup>1</sup>

<sup>1</sup>*Department of Physics and Astronomy, Interdisciplinary Nanoscience Center, Aarhus University, 8000 Aarhus C, Denmark*

<sup>2</sup>*Department of Physics, Zhejiang University, Hangzhou, 310027 China*

<sup>3</sup>*Institut für Experimentalphysik, Freie Universität Berlin, 14195 Berlin, Germany*

<sup>4</sup>*Fachbereich Physik, Freie Universität Berlin, 14195 Berlin, Germany*

<sup>5</sup>*Departamento de Física de la Materia Condensada,  
EHU/UPV, Barrio Sarriena sn 48940 Leioa, Spain.*

<sup>6</sup>*Donostia International Physics Center (DIPC),  
Paseo Manuel de Lardizabal, 4. 20018 Donostia-San Sebastian, Spain.*

(Dated: December 4, 2018)

The electronic structure of Sb(110) is studied by angle-resolved photoemission spectroscopy and first-principle calculations, revealing several electronic surface states in the projected bulk band gaps around the Fermi energy. The dispersion of the states can be interpreted in terms of a strong spin-orbit splitting. The bulk band structure of Sb has the characteristics of a strong topological insulator with a  $\mathbb{Z}_2$  invariant  $\nu_0 = 1$ . This puts constraints on the existence of metallic surface states and the expected topology of the surface Fermi contour. However, bulk Sb is a semimetal, not an insulator and these constraints are therefore partly relaxed. This relation of bulk topology and expected surface state dispersion for semimetals is discussed.

PACS numbers: 73.20.At, 71.10.Ca, 79.60.Bm

## INTRODUCTION

Topological insulators are a recently discovered class of materials with fascinating properties: while the inside of the solid is insulating, fundamental topological considerations require the surfaces to be metallic [1–6]. The metallic surface states show an unconventional spin texture [7, 8] and electron dynamics [9–11]. They are furthermore stable in the sense that their existence is a bulk property and derived from the bulk electronic structure. The surface state spectrum can be predicted by the single  $\mathbb{Z}_2$  invariant  $\nu_0$ . For  $\nu_0 = 1$  the bulk electronic structure is that of a strong topological insulator and gap-less, stable surface states are expected whereas this is not the case for  $\nu_0 = 0$  [1, 2].

The topology of the bulk bands does not only permit the prediction of metallic surface states, it also puts rigorous constraints on the number of the bands crossing the Fermi energy in certain high-symmetry directions, and even on the number of closed Fermi contours encircling high-symmetry points [1, 2]. These topological predictions were found to be obeyed for the (111) surface of the three dimensional topological insulators  $\text{Bi}_{1-x}\text{Sb}_x$  ( $0.09 < x < 0.18$ ) [1, 4, 7], as well as  $\text{Bi}_2\text{Se}_3$  and  $\text{Bi}_2\text{Te}_3$  [12–16].

The surface electronic structure of the group V semimetals bismuth and antimony is very similar to that of the topological insulator  $\text{Bi}_{1-x}\text{Sb}_x$ . The similarity to the corresponding Bi surfaces is not surprising since  $x$  is quite small. Indeed, all Bi surfaces studied so far have been found to support metallic electronic states, in contrast to the semimetallic bulk [17–20]. It has been

suggested [18] and later shown that these surface states are split by the spin-orbit interaction [21] and the Bi surface states were found to show some characteristics that were later discussed in connection with the topological insulators, such as the absence of back-scattering [22] or the fact that charge density waves cannot be formed even for nested Fermi contours [23]. The similarity  $\text{Bi}_{1-x}\text{Sb}_x$  to pure Sb is that the gapped alloy inherits its topological character from Sb ( $\nu_0 = 1$ ), not from Bi ( $\nu_0 = 0$ ). Thus, Sb has the characteristics of a strong topological insulator while it is a semimetal, not an insulator. Experimental electronic structure results have so far only been reported for the Sb(111) surface [7, 24].

In this paper we present results from the electronic structure of Sb(110). This surface is interesting for two reasons. The first is the non-trivial bulk topology of Sb. The second is that, compared to to the (111) surface, (110) has more distinct so-called time-reversal invariant momenta (four instead of two) and this provides the opportunity to study the surface state topology in more detail.

An interesting question is what the bulk topological considerations imply for the semimetal surfaces. Strictly spoken, there is no fundamental reason to expect metallic surface states on Bi or Sb but such states have so-far always been found and appear to be quite robust. For Sb(110), we argue that while the semimetallic character of the substrate inhibits a statement on the global existence of surface states, the dispersion of states in certain high-symmetry directions of  $k$ -space (directions without bulk projected states) can still be rigorously compared to topological predictions.

Figure 1 provides an overview of the Sb(110) surface

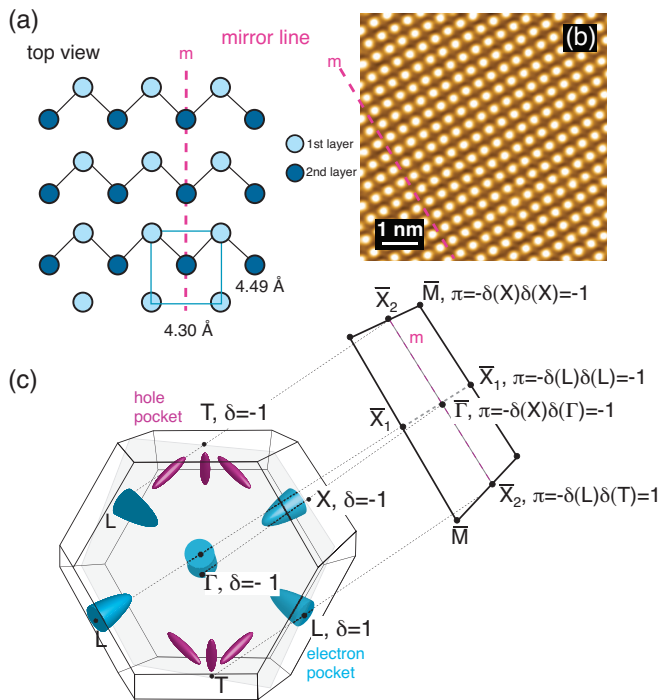


FIG. 1: (Color online) (a) Truncated-bulk geometric structure of Sb(110). (b) STM topography of the surface. (c) Bulk Brillouin zone of Sb with a sketch of the Fermi surface elements (qualitatively and not to scale), together with a projection onto the Sb(110) surface Brillouin zone. The grey plane is a bulk mirror plane which projects onto a surface mirror line. For the 8 bulk time-reversal invariant momenta (TRIMs)  $\Gamma_i$ , the parity invariants  $\delta(\Gamma_i)$  are given. These are projected onto the 4 surface TRIMs  $\lambda_a$ , resulting in the surface fermion parity  $\pi(\lambda_a) = -\delta(\Gamma_i)\delta(\Gamma_j)$ . The resulting values of  $\pi(\lambda_a)$  are denoted at the surface TRIMs [26].

in real and reciprocal space. Figure 1(a) and (b) show a model of the truncated bulk surface and the STM topography [25], respectively. Neither STM nor low energy diffraction give any indication of a surface reconstruction. Figure 1(c) illustrates the bulk Brillouin zone of Sb with the bulk Fermi surface and the projection of the former onto the (110) surface. A remarkable feature of the Sb(110) surface is its low symmetry with a mirror line being the only symmetry element. Nevertheless, time-reversal symmetry guarantees the electronic structure for high symmetry points such as  $\bar{M}$  to be the same for all four equivalent points [18], effectively giving rise to a second mirror symmetry in the observed band dispersion.

## EXPERIMENTAL AND THEORETICAL METHODS

We have investigated the surface electronic structure of Sb(110) using angle-resolved photoemission (ARPES).

Data were taken at the SGM-III beamline of the synchrotron radiation facility ASTRID in Aarhus [27]. The combined energy and angular resolution was better than 10 meV and  $0.13^\circ$ , respectively. The data shown here were all taken using a photon energy of 20 eV. The Sb(110) surface was cleaned *in situ* by cycles of sputtering and annealing to 520 K. The clean surface showed a  $(1 \times 1)$  low energy electron diffraction pattern with the only symmetry being the mirror line that defines the  $\bar{\Gamma}\bar{X}_2$  direction of surface Brillouin zone [28]. During the photoemission measurements the sample was kept at a temperature of 60 K. We have also studied the surface topology using scanning tunneling microscopy (STM) at 5 K.

The Sb(110) surface was modeled considering a repeated slab system consisting of 54 layers, relaxed up to forces  $< 10^{-4}$  Ry/a.u. We used fully relativistic norm-conserving pseudopotentials as described in Ref. [29], with the energy cutoff corresponding to  $E_c=60$  Ry. We considered the Perdew-Burke-Ernzerhof implementation [30] of the generalized gradient approximation within a non-collinear implementation of density functional theory (DFT) [29, 31]. The self consistent DFT cycle was completed with a  $20 \times 20$  Monkhorst-Pack mesh. In order to calculate the projection of the bulk band structure onto the (110) surface, we have also used the tight-binding scheme of Liu and Allen [32]. This is expected to give reliable results very close to the Fermi energy since the tight-binding parameters have been determined to reproduce the essential features of the bulk Fermi surface.

## RESULTS

The results of the ARPES investigation are shown in Figs. 2 and 3. The figures show the photoemission intensity at the Fermi level and as a function of binding energy along some high-symmetry directions, respectively. For clarity, both figures show two versions of the data: only the measured intensity and this intensity superimposed with colored lines to guide the eye for identifying the surface states and the projected bulk band structure. Note that the colored lines are only drawn where the data shows clearly identifiable structures; they are not representation of the actual Fermi contour or dispersion that is expected to continue even if the colored lines end.

The Fermi contour in Figure 2 shows several surface-related features, identified by their location outside the projected band continuum and the fact that their position is insensitive to the photon energy used. Most pronounced are a circular contour around  $\bar{M}$  (outlined in red) and a butterfly-like feature that encloses the  $\bar{X}_1$  point (blue). Two smaller pockets are seen along the  $\bar{M}\bar{X}_2$  line (light blue) and the  $\bar{X}_2\bar{\Gamma}$  line (green). The latter falls partly into the bulk continuum and thus has the character of a surface resonance there. Finally, we find a

faint trace split off the ‘butterfly wing’ and dispersing towards  $\bar{X}_2$  (magenta) and some faint intensity crossing the  $\bar{X}_2\bar{\Gamma}$  line (also magenta). As we shall see later from the calculated electronic structures, these features are probably joint to form a large hole pocket around  $\bar{\Gamma}$ , but this is not clearly seen in the data.

The detailed character of the features emerges from the dispersion shown in Figure 3. The circular contour around  $\bar{M}$  (red) is a hole pocket whereas the feature along  $\bar{M}\bar{X}_2$  (light blue) is a shallow electron pocket. The two features can be interpreted as spin-orbit split partners stemming from the same state. The state is unoccupied and assumed to be spin-degenerate at  $\bar{M}$ , but split away from this point. One of the split bands disperses steeply downwards and forms the hole pocket. The other one forms the electron pocket along  $\bar{M}\bar{X}_2$ . At  $\bar{X}_1$  the surface state is also two-fold degenerate but it is occupied and can thus be observed by ARPES. Away from  $\bar{X}_1$  the state clearly splits into two bands, both along  $\bar{X}_1\bar{M}$  and  $\bar{X}_1\bar{\Gamma}$ , but these bands merge again and are too close to be distinguished at the Fermi level crossings along these high-symmetry directions. Consequently, the Fermi level crossings along  $\bar{X}_1\bar{\Gamma}$  and  $\bar{X}_1\bar{M}$  are double crossings. Close to the  $\bar{X}_1\bar{M}$  direction the two bands forming the double crossing separate into the circle and the butterfly.

The weakest features in the data is the band which splits off from the butterfly structure and disperses towards  $\bar{X}_2$  (magenta). Its presence is clearly required by the overall Fermi contour topology: the two spin-split surface state branches are occupied at  $\bar{X}_1$  and empty at  $\bar{M}$  and  $\bar{\Gamma}$ . Consequently, two Fermi level crossings have to be found along the corresponding high-symmetry lines. Along the  $\bar{X}_1\bar{M}$  direction, the two crossings are formed by the circular contour around  $\bar{M}$  and the ‘wing’ of the butterfly, which is non-degenerate. Along  $\bar{X}_1\bar{\Gamma}$ , the blue feature is two-fold degenerate. The weak magenta feature correspond to the second Fermi level crossing. As it disperses away from the butterfly, its intensity diminishes so much that it cannot be established whether it continues to the  $\bar{X}_2\bar{\Gamma}$  line and merges with the other magenta feature observed there, or if it merges into the projected bulk bands close to  $\bar{X}_2$ .

The identification of the electronic structure near the  $\bar{X}_2\bar{\Gamma}$  line is more difficult due to the presence of bulk states. As pointed out above, the feature outlined in green appears to be a closed pocket around this line but it falls partly into the bulk continuum. Also, only the band giving rise to the crossing nearest to  $\bar{X}_2$  is clearly identifiable in the dispersion, the crossing further away from  $\bar{X}_2$  is very weak and the dispersion cannot be followed to higher binding energies. Nevertheless, the dispersion of the first band suggests that the pocket is a hole pocket. The magenta feature is well-separated from the bulk continuum at the Fermi level but it is very broad and its dispersion is only clearly observed near  $E_F$ . The sign of its group velocity would be consistent with the

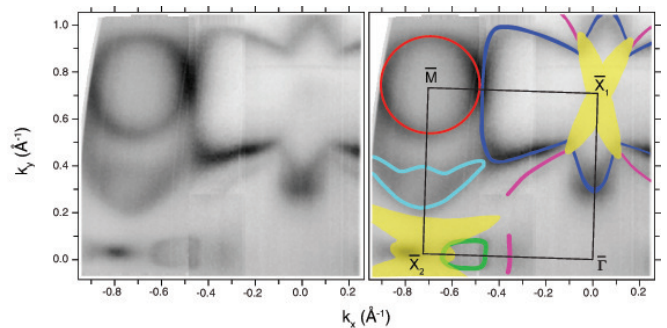


FIG. 2: (Color online) Photoemission intensity at the Fermi level. Dark corresponds to high intensity and the dark features outside the projected bulk band continuum are interpreted as the surface Fermi contour. The left part of the figure shows the raw data whereas the different structures are indicated by colored lines as a guide to the eye on the right part. Different colors are used for different surface state features. The light yellow areas correspond to the projected bulk Fermi surface (states within  $\pm 5$  meV of the Fermi energy), calculated using the tight-binding parameters from Liu and Allen [32].

feature being part of a hole pocket around  $\bar{\Gamma}$ .

The calculated Fermi contour and surface state dispersion is given in Fig. 4. Overall, a very good agreement with the experimental findings is obtained, especially considering the small energy scale of the bands (a few hundred meV) and the fact that self-energy effects are not incorporated. In fact, the main features of the measured Fermi contour are immediately recognized, especially the butterfly close to  $\bar{X}_1$  and the hole pocket around  $\bar{M}$ . The calculation also confirms the interpretation of the surface states as being non-degenerate spin-split bands that are degenerate only at points where this degeneracy is enforced by symmetry (so-called time-reversal invariant momenta, see below).

Some smaller details are not entirely captured by the theoretical results. First, the very shallow electron pocket along  $\bar{M}\bar{X}_2$  appears in the calculations as a dip in the dispersion of the band, which does not cross the Fermi level. This can easily be accounted for by small uncertainties in the calculations, like for example, a slight error in the position of the Fermi level or in the shape of the band dispersion. The second apparent difference between experiment and theory is the presence of a large hole pocket encircling the  $\bar{\Gamma}$  point in the latter. However, a slightly higher Fermi energy in the theory would cause the hole pocket to merge with the butterfly structure, giving rise to the experimentally observed double crossing on the  $\bar{\Gamma}\bar{X}_1$  line and to the weak structure split off the butterfly when going from this line towards  $\bar{M}$ . In fact, merging the magenta structures in Fig. 2 would give rise to a large electron pocket around  $\bar{\Gamma}$  and it seems likely that the lines should be merged since an open Fermi

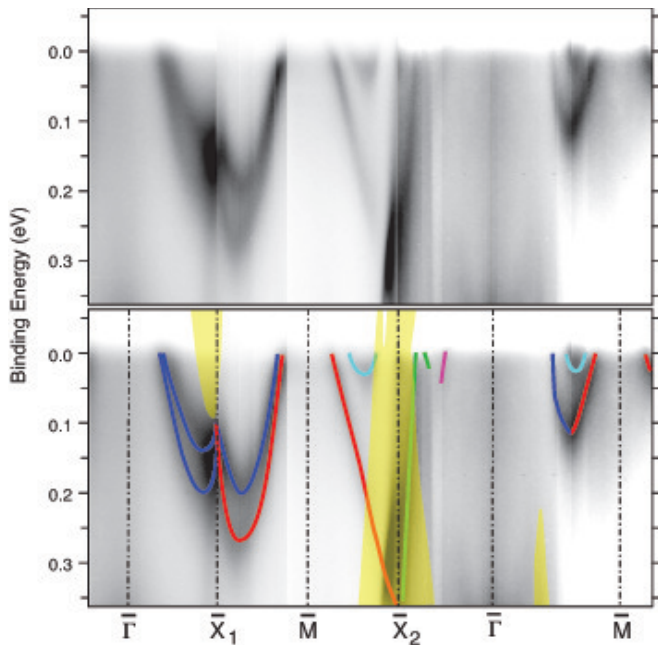


FIG. 3: (Color online) Photoemission intensity as a function of binding energy along different directions of the surface Brillouin zone. The upper part shows the raw data. In the lower part, the observed bands are emphasized by colored lines. The colors are corresponding to those used in Figure 2. The light yellow areas represent the projected bulk band structure.

contour would be unphysical.

As far as the surface state dispersion is concerned, we can thus draw the following conclusions: the electronic structure of Sb(110) shows several electronic surface states crossing the Fermi level. It thus has the character of a good metal in contrast to the semimetallic bulk. This appears to be a general feature of the Bi and Sb semimetal surfaces and it has been explained as resulting from the combination of symmetry breaking and a strong spin-orbit interaction [18, 20, 21, 24, 33]. The electronic structure of Sb(110) is similar to that of Bi(110) in some parts of the surface Brillouin zone. The observed and calculated dispersion is mostly consistent with the expected degeneracy at high symmetry points (see below) and a spin-orbit splitting away from these points. While we do not directly measure the spin of the bands, this interpretation appears to be based on solid ground. It is consistent with the findings on all other Bi, Sb and  $\text{Bi}_{1-x}\text{Sb}_x$  surfaces and with the calculations reported here. Moreover, the spin-split nature of the states is also confirmed by the absence of the characteristic back-scattering standing waves in our STM investigations [34]. Compared to Bi(110), the spin-orbit splitting is smaller, as expected. This has the interesting consequence of concentrating the spin-orbit split bands in an even narrower window around the Fermi energy, presumably leading to a higher density of states there,

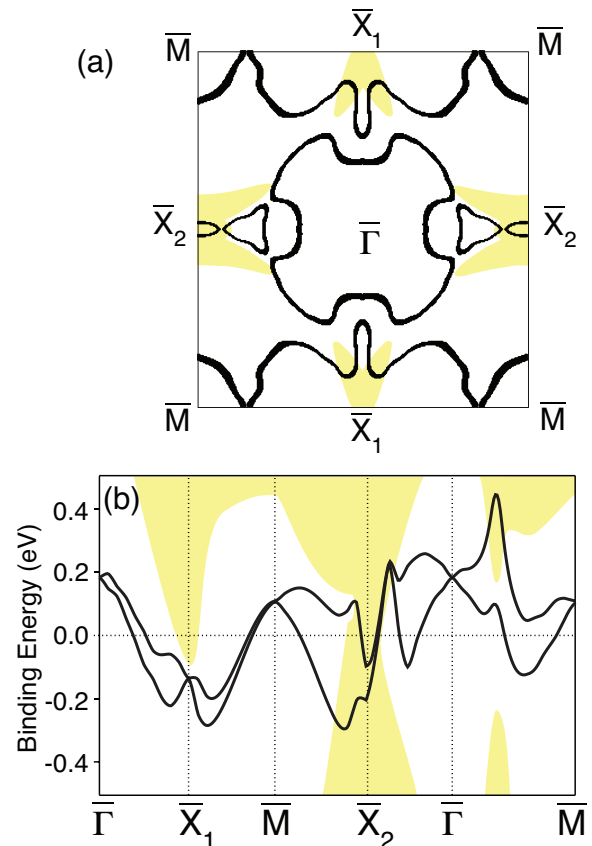


FIG. 4: (Color online) (a) Calculated Fermi contour and (b) surface state dispersion. The lines represent the surface states from the DFT slab calculation. The yellow continuum is the projected bulk band structure calculated using the tight-binding parameters from Liu and Allen [32].

and possibly opening the option of tuning the electronic structure as to purposefully move van Hove singularities to the Fermi level [35, 36].

## DISCUSSION

We now turn back to the more general question of how much topological considerations affect the existence of surface states on semimetal surfaces. We discuss this using the specific example of Sb(110) but we also address other surface orientations and the case of Bi.

The topological situation for materials with inversion symmetry in general and Bi, Sb and  $\text{Bi}_{1-x}\text{Sb}_x$  in particular has been studied in great detail by Teo, Fu and Kane [26] and we summarize some of their results here. The  $\mathbb{Z}_2$  invariant  $\nu_0$  which dictates the topological character

of the solid is given by

$$(-1)^{\nu_0} = \prod_{n=1}^8 \delta_i \quad (1)$$

where the  $\delta_i$  are the parity invariants of the eight bulk time-reversal invariant momenta (TRIMs)  $\Gamma_i$ , defined by  $-\Gamma_i = \Gamma_i + G$  where  $G$  is a bulk reciprocal lattice vector. For bulk Sb, the TRIMs are  $\Gamma$ , T, L and X. Their  $\delta_i$  values are calculated by

$$\delta(\Gamma_i) = \prod_{n=1} \xi_{2n}(\Gamma_i) \quad (2)$$

where the  $\xi_{2n}(\Gamma_i) = \pm 1$  are the parity eigenvalues of the  $2n$ th occupied band at  $\Gamma_i$ , obtained from a bulk band structure calculation [32, 37]. The  $\delta_i$  values for the bulk TRIMs are given in Figure 1(c). The key-difference between Bi on one hand and  $\text{Bi}_{1-x}\text{Sb}_x$  or Sb on the other hand is that  $\nu_0 = 0$  for the former and 1 for the latter. This stems from a single change of a parity invariant  $\delta(L)$  from  $-1$  in Bi to 1 in the other compounds (see Table I in Ref. [26]).

The bulk parity invariants can now be used to describe fundamental properties of the surface electronic structure. To do this, the surface TRIMs  $\Lambda_a$  are defined such that  $\Lambda_a = -\Lambda_a + g$  where  $g$  is a surface reciprocal lattice vector. For these points ( $\bar{\Gamma}$ ,  $\bar{M}$ ,  $\bar{X}_1$  and  $\bar{X}_2$ ), the surface state bands must be spin-degenerate, even in the presence of a strong spin-orbit interaction. For each surface TRIM, the so-called surface fermion parity  $\pi_i$  can be determined. Essentially,  $\pi_i$  is obtained by projecting out the bulk parity invariants onto the corresponding surface TRIMs (see Figure 1(c)), using the relation  $\pi(\Lambda_a) = -\delta(\Gamma_i)\delta(\Gamma_j)$  [26]. For instance,  $\pi$  for  $\bar{\Gamma}$  has to be calculated from the parity invariants of the bulk  $\Gamma$  and X points, which are both  $-1$  and hence  $\pi(\bar{\Gamma}) = -1$ . As mentioned above, the only difference in bulk parity invariants between Bi and Sb is at the L point where  $\delta(L) = -1$  and 1 for Bi and Sb, respectively, and this difference implies change the surface fermion parity at  $\bar{X}_2$  from  $-1$  to 1.

The surface fermion parity in Figure 1(c) can be used to predict the number of closed Fermi contours around a surface TRIM or the number of Fermi level crossings between two surface TRIMs. We start with the latter prediction which is easier to verify experimentally. The number of crossings has to be zero or even if the two surface TRIMs have the same parity and odd otherwise. Based on these rules, Teo, Fu and Kane [26] have made detailed predictions of the qualitative surface electronic structure of many surfaces. We adopt their result for  $\text{Bi}_{1-x}\text{Sb}_x$  to the topologically identical case of Sb(110) and find that there must be an odd number of Fermi level crossings between  $\bar{X}_2$  and any other surface TRIM and an even number between two surface TRIMs not involving  $\bar{X}_2$ .

An inspection of Figs. 2, 3 shows that this is the case, despite of the presence of bulk Fermi surface projections. The situation is clearest for the  $\bar{X}_1$  point. At  $\bar{X}_1$  we find the two states to be degenerate, as predicted, and in both the  $\bar{X}_1\bar{\Gamma}$  and  $\bar{X}_1\bar{M}$  direction we find two Fermi level crossings, also agreeing with the prediction.

For  $\bar{X}_2$  the situation is difficult to determine solely on the basis of our experiments, because the intensity of the surface bands close to this point is very weak, due to the presence of the bulk band continuum. At first glance, the number of Fermi level crossings seems to be as predicted from the topological arguments: along both directions,  $\bar{M}\bar{X}_2$  and  $\bar{X}_2\bar{\Gamma}$ , we can identify one closed contour plus an extra crossing, and thus an odd number of crossings.

We can also compare the experimentally observed number of closed Fermi contours around each surface TRIM to the topological predictions based on the surface fermion parity. A surface TRIM with  $\pi(\Lambda_a) = -1$  is expected to be encircled by an odd number of Fermi contours while the number is zero or even for  $\pi(\Lambda_a) = 1$ . Thus, we expect an odd number of contours around  $\bar{\Gamma}$ ,  $\bar{M}$  and  $\bar{X}_1$  and an even number around  $\bar{X}_2$ . For  $\bar{M}$  this is fulfilled, as the point is encircled by one hole pocket.  $\bar{X}_1$  is also encircled by only one contour, which is consistent with  $\pi = 1$ . For  $\bar{\Gamma}$  the situation is unclear, as it depends on the weak feature which is split off the butterfly. It is likely that this feature connects to the observed crossing along the  $\bar{X}_2\bar{\Gamma}$  line, giving rise to a circular contour around  $\bar{\Gamma}$ , as also suggested by our calculation. For  $\bar{X}_2$  the situation is again obscured due to the projected bands around this point and it is difficult to determine whether this state is encircled by any closed Fermi contour.

The situation becomes clearer when we look at the calculated electronic structure and test it against the topological predictions. For  $\bar{\Gamma}$ ,  $\bar{M}$  and  $\bar{X}_1$  and the lines between these points, the number of closed contours and Fermi level crossings are as expected. For  $\bar{X}_2$ , however, the topological predictions appear to be violated: the calculations show an additional closed Fermi contour around this point, and thus the number of Fermi level crossings between  $\bar{X}_2$  and any other TRIM becomes even, not odd as predicted. The origin of this discrepancy is that the states lie within the bulk continuum and are thus not surface states anymore. In fact, the calculations find that the surface band is mixed with bulk states and penetrates deeply into the bulk of the slab. This is also responsible for the apparent lifting of the degeneracy at  $\bar{X}_2$  (thinner slabs give a bigger splitting). The deep penetration of surface bands into the bulk breaks down the validity of surface fermion parity rules and, hence, the predictions of the topological theory, which can only be strictly applied for insulators.

We address this issue in more detail and ask to what degree topological arguments can be used to make firm predictions as to the surface state dispersion on semimetal surfaces. In a simple picture, the need for an



odd number of Fermi level crossings between two surface TRIMs arises because of their different surface fermion parity. In an insulator, due to the existence of a global energy gap around  $E_F$ , the necessary parity change between surface TRIMs can only be achieved by surface states. On a semimetal, on the other hand, a surface-projected bulk state can be used for this purpose, if a projected bulk Fermi surface can be found between the two surface TRIMs in question. This argument implies that the number of  $E_F$  crossings between TRIMs without any projected Fermi surface in between them should be as topologically predicted. For Sb(110) the only such connection is between  $\bar{\Gamma}$  and  $\bar{M}$  and this cut does indeed show an even number of surface Fermi level crossings, as predicted. Similar arguments can be made for the  $\bar{X}_1\bar{\Gamma}$  and  $\bar{X}_1\bar{M}$  directions. Here there is a bulk Fermi surface projection (at  $\bar{X}_1$ ) but the surface state dispersion lies completely outside this projection and consequently it is also in accordance with the topological predictions. In all these situations, we only observe an even number of Fermi level crossings between two TRIMs and thus a topologically trivial situation. Forcing a semimetal surface to be metallic in a topological sense would require an odd number of crossings between two TRIMs without a projected bulk Fermi surface element in between. There is no obvious candidate for such a situation among the low-index surface of Bi and Sb.

Concluding, we have presented experimental and theoretical results on the electronic structure of Sb(110), a non-(111) surface of a topologically non-trivial material. Along the directions connecting TRIMs without any bulk Fermi surface contribution, the observed band dispersion is in excellent agreement with the predictions of the surface bands topology. The topological arguments become invalid if the projected bulk Fermi surface is present and the surface bands are allowed to mix with the bulk states.

The authors gratefully acknowledge stimulating discussions with Charles Kane, Hugo Dil and Jürg Osterwalder, as well as support by the Danish Council for Independent Research - Natural Sciences, the Deutsche Forschungsgemeinschaft (STR 1151/1-1) and the Spanish Ministry of Science and Innovation (FIS2010-19609-C02-00).

---

[1] L. Fu and C. L. Kane, Phys. Rev. B **76**, 045302 (2007).  
 [2] L. Fu, C. L. Kane, and E. J. Mele, Phys. Rev. Lett. **98**, 106803 (2007).  
 [3] J. E. Moore and L. Balents, Phys. Rev. B **75**, 121306 (2007).  
 [4] D. Hsieh, D. Qian, L. Wray, Y. Xia, Y. S. Hor, R. J. Cava, and M. Z. Hasan, Nature **452**, 970 (2008).  
 [5] S. C. Zhang, Physics **1**, 6 (2008).  
 [6] J. E. Moore, Nature **464**, 194 (2010).  
 [7] D. Hsieh, Y. Xia, L. Wray, D. Qian, A. Pal, J. H. Dil, J. Osterwalder, F. Meier, G. Bihlmayer, C. L. Kane, *et al.*,

Science **323**, 919 (2009).  
 [8] D. Hsieh, Y. Xia, D. Qian, L. Wray, F. Meier, J. H. Dil, J. Osterwalder, L. Patthey, A. V. Fedorov, H. Lin, *et al.*, Phys. Rev. Lett. **103**, 146401 (2009).  
 [9] M. König, S. Wiedmann, C. Brune, A. Roth, H. Buhmann, L. W. Molenkamp, X.-L. Qi, and S.-C. Zhang, Science **318**, 766 (2007).  
 [10] P. Roushan, J. Seo, C. V. Parker, Y. S. Hor, D. Hsieh, D. Qian, A. Richardella, M. Z. Hasan, R. J. Cava, and A. Yazdani, Nature **460**, 1106 (2009).  
 [11] Z. Alpichshev, J. G. Analytis, J.-H. Chu, I. R. Fisher, Y. L. Chen, Z. X. Shen, A. Fang, and A. Kapitulnik, Phys. Rev. Lett. **104**, 016401 (2010).  
 [12] H. Zhang, C.-X. Liu, X.-L. Qi, X. Dai, Z. Fang, and S.-C. Zhang, Nature Physics **5**, 438 (2009).  
 [13] Y. Xia, D. Qian, D. Hsieh, L. Wray, A. Pal, H. Lin, A. Bansil, D. Grauer, Y. S. Hor, R. J. Cava, *et al.*, Nature Physics **5**, 398 (2009).  
 [14] H.-J. Noh, H. Koh, S.-J. Oh, J.-H. Park, H.-D. Kim, J. D. Rameau, T. Valla, T. E. Kidd, P. D. Johnson, Y. Hu, *et al.*, EPL **81**, 57006 (2008).  
 [15] Y. L. Chen, J. G. Analytis, J. H. Chu, Z. K. Liu, S. K. Mo, X. L. Qi, H. J. Zhang, D. H. Lu, X. Dai, Z. Fang, *et al.*, Science **325**, 178 (2009).  
 [16] D. Hsieh, Y. Xia, D. Qian, L. Wray, J. H. Dil, F. Meier, J. Osterwalder, L. Patthey, J. G. Checkelsky, N. P. Ong, *et al.*, Nature **460**, 1101 (2009).  
 [17] C. R. Ast and H. Höchst, Phys. Rev. Lett. **87**, 177602 (2001).  
 [18] S. Agergaard, C. Søndergaard, H. Li, M. B. Nielsen, S. V. Hoffmann, Z. Li, and Ph. Hofmann, New J. Phys. **3**, 15.1 (2001).  
 [19] Ph. Hofmann, J. E. Gayone, G. Bihlmayer, Y. M. Koroteev, and E. V. Chulkov, Phys. Rev. B **71**, 195413 (2005).  
 [20] J. W. Wells, J. H. Dil, F. Meier, J. Lobo-Checa, V. N. Petrov, J. Osterwalder, M. M. Ugeda, I. Fernandez-Torrente, J. I. Pascual, E. D. L. Rienks, *et al.*, Phys. Rev. Lett. **102**, 096802 (2009).  
 [21] Y. M. Koroteev, G. Bihlmayer, J. E. Gayone, E. V. Chulkov, S. Blügel, P. M. Echenique, and Ph. Hofmann, Phys. Rev. Lett. **93**, 046403 (2004).  
 [22] J. I. Pascual, G. Bihlmayer, Y. M. Koroteev, H. P. Rust, G. Ceballos, M. Hansmann, K. Horn, E. V. Chulkov, S. Blugel, P. M. Echenique, *et al.*, Phys. Rev. Lett. **93**, 196802 (2004).  
 [23] T. K. Kim, J. Wells, C. Kirkegaard, Z. Li, S. V. Hoffmann, J. E. Gayone, I. Fernandez-Torrente, P. Haberle, J. I. Pascual, K. T. Moore, *et al.*, Phys. Rev. B **72**, 085440 (2005).  
 [24] K. Sugawara, T. Sato, S. Souma, T. Takahashi, M. Arai, and T. Sasaki, Phys. Rev. Lett. **96**, 046411 (2006).  
 [25] I. Horcas, R. Fernandez, J. M. Gomez-Rodriguez, J. Colchero, J. Gomez-Herrero, and A.M. Baro, Rev. Sci. Inst. **78**, 013705 (2007).  
 [26] J. C. Y. Teo, L. Fu, and C. L. Kane, Phys. Rev. B **78**, 045426 (2008).  
 [27] S. V. Hoffmann, C. Søndergaard, C. Schultz, Z. Li, and Ph. Hofmann, Nuclear Inst. and Methods in Physics Research A **523**, 441 (2004).  
 [28] J. Sun, A. Mikkelsen, M. F. Jensen, Y. M. Koroteev, G. Bihlmayer, E. V. Chulkov, D. L. Adams, Ph. Hofmann, and K. Pohl, Phys. Rev. B **74**, 245406 (2006).  
 [29] A. D. Corso and A. M. Conte, Phys. Rev. B **71**, 115106 (2005).

- [30] J. P. Perdew, K. Burke, and M. Ernzerhof, Phys. Rev. Lett. **77**, 3865 (1996).
- [31] [www.pwscf.org](http://www.pwscf.org).
- [32] Y. Liu and R. E. Allen, Phys. Rev. B **52**, 1566 (1995).
- [33] Ph. Hofmann, Prog. Surf. Sci. **81**, 191 (2006).
- [34] A. Stróżecka *et al.*, *to be submitted*.
- [35] C. R. Ast, J. Henk, A. Ernst, L. Moreschini, M. C. Falub, D. Pacile, P. Bruno, K. Kern, and M. Grioni, Phys. Rev. Lett. **98**, 186807 (2007).
- [36] C. R. Ast, D. Pacile, L. Moreschini, M. C. Falub, M. Papagno, K. Kern, M. Grioni, J. Henk, A. Ernst, S. Ostanin, *et al.*, Phys. Rev. B **77**, 081407 (2008).
- [37] L. M. Falicov and P. J. Lin, Phys. Rev. **141**, 562 (1966).